J Mater Sci (2010) 45:3990–3997
DOI 10.1007/s10853-010-4471-y

Creep behavior of MAR-M 302 Co-base superalloy

M. Aghaie-Khafri · B. Binesh

Received: 7 October 2009 / Accepted: 5 April 2010 / Published online: 22 April 2010

Abstract MAR-M 302 a Co-base superalloy is currently used for nozzle guide vanes and stator blades in military and commercial aircraft-turbine engines. These components are usually operated at 1073–1273 K. In this study, the uniaxial constant load creep behavior of MAR-M 302 superalloy over temperature range of 1088–1198 K and stress range of 155–321 MPa was investigated. Concerning creep as thermally activated phenomenon, the investigated alloy followed empirical equation $\dot{\varepsilon} = A\sigma^n \exp\left(-\frac{Q}{RT}\right)$ with n values ranging mainly from 7 to 10. The mean apparent activation energy was calculated as 525 ± 29 kJ/mol. The correlation between rupture life and creep characteristics was studied by different prediction methods that are based on the iso-stress lines and those relating the secondary or steady state creep rate to rupture life.

Introduction

Cobalt-base alloys emerge as the first true members of the superalloy family. The initial applications involved cast compositions for use as blades in turbo-superchargers for piston engines in 1930s, then as blades and vanes in the first gas turbine engines of 1940s. The use of cast cobalt-base alloys survives in current gas turbine engines mainly as nozzle guide vanes and stator blades [1]. Cobalt-base alloys are also widely used as artificial knee, to a lesser extent, as implants that fix bone fractures, that is, bone screws, staples, and plates [2]. Development and utilization of cobalt-base alloys were greatly overshadowed by the advent of the nickel-base superalloys. However, cast and wrought cobalt-base alloys continued to be used for the following primary reasons. (1) Cobalt alloys exhibit higher melting temperatures and suitable creep properties, providing useful stress capability to a higher absolute temperature than nickel- or iron-base alloys. (2) They offer superior hot-corrosion resistance to contaminated gas turbine atmospheres due to their higher chromium contents. (3) In general, cobalt alloys exhibit superior thermal fatigue resistance and weldability than nickel alloys [3–5].

Cobalt-base superalloys, unlike other superalloys, are not strengthened by a coherent, ordered precipitate. Rather, they are characterized by a solid solution strengthened austenitic fcc matrix in which a variety of carbides, mainly coarse primary $M_{23}C_6$, M_6C, and MC carbides are distributed [6, 7]. The carbides provide strong inhibition to grain boundary sliding and grain growth as well as an impedance to dislocation mobility [8]. Unlike nickel-base alloys, which have a high tolerance for alloying elements in solid solution, cobalt-base alloys are more likely to precipitate undesirable platelike σ, Laves, and similar topologically close packed (TCP) phases [3].

High temperature components can be life limited by creep damage under thermomechanical loading. In general, creep involves the time dependent deformation and fracture of materials [9]; furthermore, it is accelerated by an increase in stress or temperature. Over the past several decades, considerable efforts have been made to gain a fundamental understanding of creep mechanisms and to develop engineering design criterion for high temperature components [10, 11].

M. Aghaie-Khafri (✉) · B. Binesh
Faculty of Mechanical Engineering, K.N. Toosi University of Technology, P.O. Box 19395-1999, Tehran, Iran
e-mail: maghaei@kntu.ac.ir

MAR-M 302 is a cobalt-base casting superalloy, possessing good high temperature creep properties and excellent resistance to oxidation and corrosion in severely aggressive environments. This material has found widespread applications in gas turbine engine components like blades, vanes, and combustion chambers. A review of the evolutionary of wrought cobalt-base alloys in terms of alloy design and physical metallurgy has been provided by Klarstrom [1]. Tensile strengths and 1000-h rupture strengths of MAR-M 302 at different temperatures together with basic physical properties of the alloy are available [2, 3]. Several studies have examined the microstructure and thermal–mechanical fatigue characteristics of MAR-M 509 [6, 12, 13]. However, little attention has been paid to creep behavior of MAR-M 302 and there is no reported study on the accelerated creep and life assessment of the alloy. The objective of this study is to investigate the accelerated creep behavior of MAR-M 302 superalloy at 1088–1198 K and also to study the correlation between rupture life and creep characteristics by different life prediction methods.

Experimental procedures

The material used in this investigation was the cast cobalt-base polycrystalline superalloy MAR-M 302 supplied by Ross and Catheral Co., UK. The chemical composition of the alloy is given in Table 1. The master alloy was vacuum-induction melted and poured into the ceramic cluster molds in a 25 kg Leybold Heraeus two-chamber vacuum-induction furnace. Vacuum during melting and casting was 1.3×10^{-3} and 1.2×10^{-2} Pa, respectively. The cluster mold arrangement was six cylindrical castings, 18 mm in diameter, and 100 mm in length around the central sprue.

Cylindrical bars, 7 mm in diameter, and 70 mm long were machined out of the cast material and then the M6 creep test specimens were prepared from the bars according to the ASTM-E8. The constant load creep tests were carried out in air at a temperature range of 1088–1198 K and a stress range of 155–321 MPa. The creep strains in the gage section were measured by a linear variable differential transformer attached to an extensometer frame which was also attached to the creep specimen. The creep tests were performed until the rupture of the specimens. The temperature was monitored by three thermocouples and maintained within about ±2 K.

Results

Microstructure

Like other cast cobalt-base superalloys, the microstructure of the as-cast MAR-M 302 mainly consists of a continuous fcc matrix and a variety of carbides, mainly coarse primary $M_{23}C_6$ and M_7C_3 carbides as shown in Fig. 1. Moreover, MC carbide is also formed in MAR-M 302 due to the addition of reactive elements such as Ta and Zr. Figure 2 shows the morphology and distribution of the carbide phases in which the chromium-rich M_7C_3 carbide

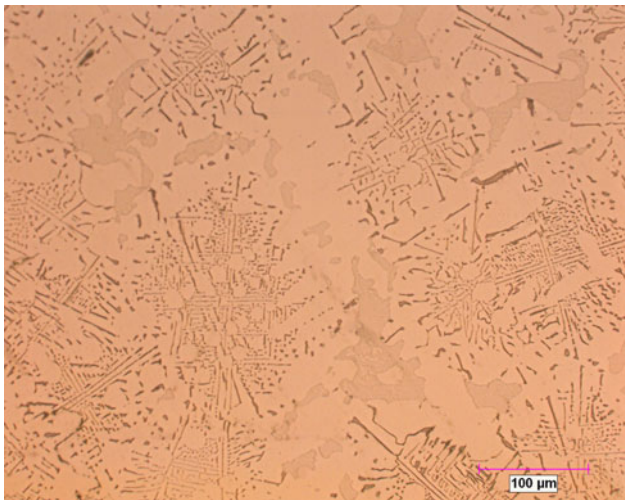

Fig. 1 Optical microstructure of the MAR-M 302 sample

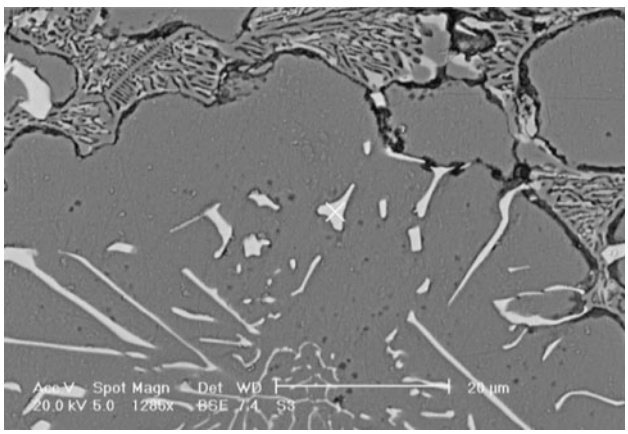

Fig. 2 Scanning electron microstructure of the MAR-M 302 sample

Table 1 Chemical composition of MAR-M 302 in wt%

	Cr	C	Fe	W	Ta	Zr	B	Zr	Co
MAR-M 302	21.503	0.850	0.501	10.062	9.021	0.204	0.006	0.040	Balance

appears dark, the MC carbide is rather light, and $M_{23}C_6$ carbide appears as a peppered constituent within grains. It is also observed that M_7C_3 carbide is in the form of irregular aggregates, while MC is present as a discrete, blocky dispersion with a Chinese script morphology, which has been observed in prior work on the MAR-M 509 alloy [3, 6].

Usually, in cast cobalt-base superalloys, secondary $M_{23}C_6$ carbide is more thermodynamically stable, and during service or exposure at high temperature, its precipitation is very common [3]. The secondary $M_{23}C_6$ precipitation is closely related to the decomposition of the primary carbides. A direct reaction mechanism for the $M_{23}C_6$ precipitation has been proposed by Jiang et al. [14]:

$$23M + 6C \rightarrow M_{23}C_6 \quad (1)$$

As a carbon reservoir, the primary carbides provided the reaction Eq. 1 with carbon atoms. Since during solidification carbon atoms were exhausted to form the primary carbides and there was little of carbon in the matrix, carbon content became a predominant factor of the $M_{23}C_6$ precipitation in the matrix [6].

Dislocations and stacking faults have a tendency to attract carbon atoms rejected by the decomposition of the primary carbides, forming a carbon segregation zone, i.e., a 'Cottrell' or 'Suzuki atmosphere [2, 6]. Therefore, secondary $M_{23}C_6$ precipitation makes a significant contribution to the mechanical property of the MAR-M 302.

Creep curves

Typical creep curves for MAR-M 302 at different test conditions are shown in Figs. 3, 4, and 5. The creep curves like most cobalt-base superalloys show three distinct regions. After the instantaneous strain, ε_0, a decelerating strain rate stage (primary creep) leads to a steady minimum creep rate, $\dot{\varepsilon}_s$ (secondary creep), which is finally followed by an accelerating stage (tertiary creep) that ends in fracture at a rupture time, t_r [6]. It is worth noting the tertiary creep leading to rupture occurs at greater rates with higher stress or temperature.

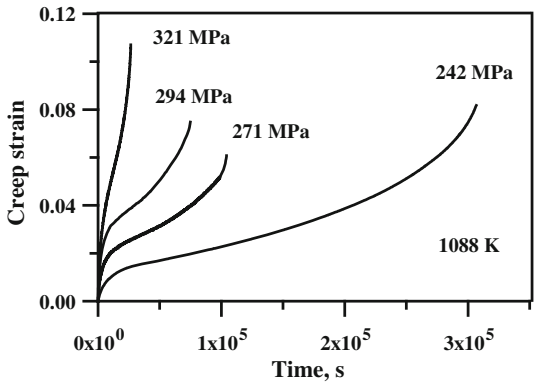

Fig. 3 Creep curves of MAR-M 302 samples at 1088 K

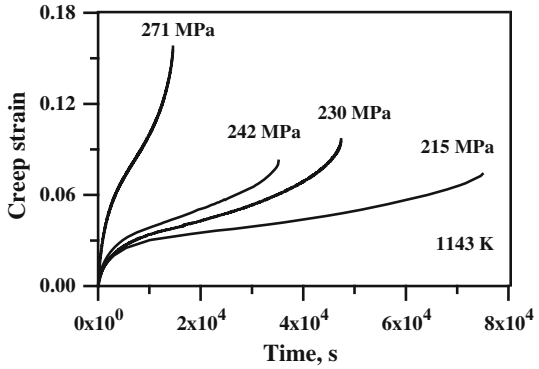

Fig. 4 Creep curves of MAR-M 302 samples at 1143 K

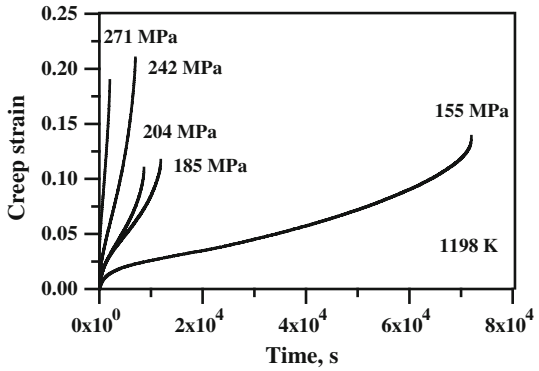

Fig. 5 Creep curves of MAR-M 302 samples at 1198 K

Figure 6 shows the microstructure of MAR-M 302 specimen after the creep test. Compared with the as-cast sample, a profusion of fine secondary precipitates were produced in the matrix and the primary carbides coarsened. Microstructural instability at elevated temperatures promotes the formation of TCP phases, such as σ, μ, or Laves phases, which are often reported to result in deterioration of stress–rupture properties [1–3]. However, no considerable TCP phases were observed in the microstructure of MAR-M 302 specimens after creep test.

As discussed previously, at high temperature the as-cast alloy was thermodynamically unstable. The primary carbides, both the M_7C_3 and MC, dissolved sluggishly and the secondary $M_{23}C_6$ carbide precipitated profusely. Consequently, during creep fine precipitation of $M_{23}C_6$ carbides takes place in the initial stage of creep in the MAR-M 302. The fine precipitation causes a significant decrease in creep rate in the transient creep region before reaching a minimum creep rate. During the stress–rupture test, other microstructural evolution also occurred and the $M_{23}C_6$ carbide coarsened. One possibility of the acceleration of

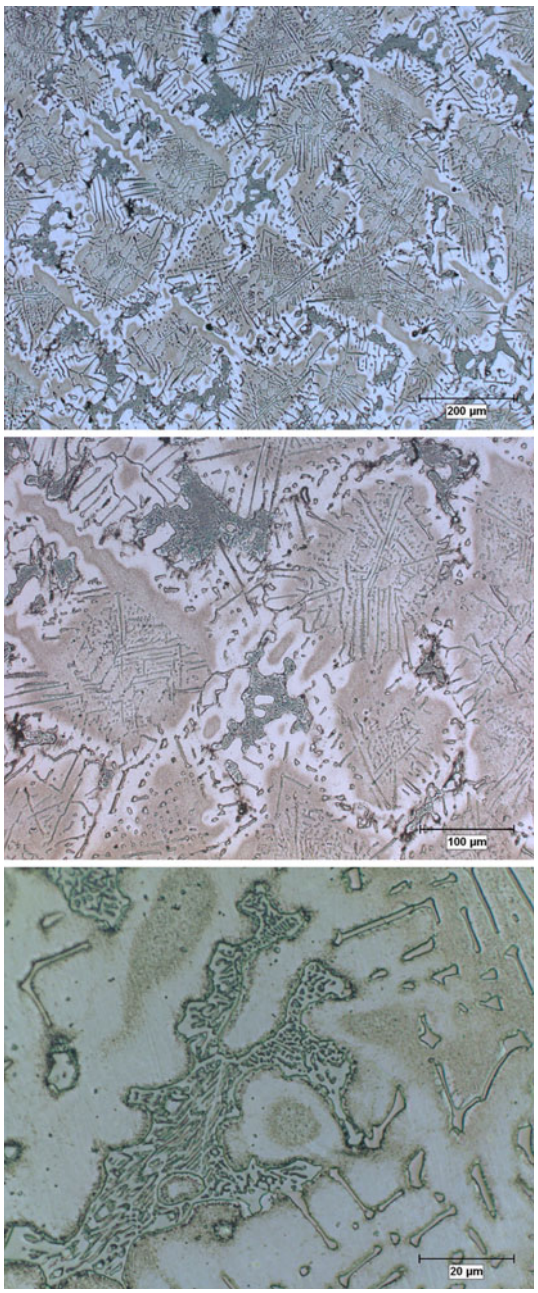

Fig. 6 Microstructure of specimens after creep test at 1088 K and 242 MPa

creep rate in the tertiary region is that coarsening of $M_{23}C_6$ carbides along grain boundaries promotes localized creep deformation in the vicinity of grain boundaries [6, 15].

Life prediction curves

At the high operating temperatures creep damage is a major life limiting factor. Thereby, the correlation between rupture life and creep characteristics was the subject of the number of studies conducted in the past which suggested some accurate methods for predicting creep life during long time, high temperature service [16]. Monkman and Grant [17] found that, for many alloy systems, the relation between the minimum creep rate $(\dot{\varepsilon}_s)$ and time to rupture (t_r) can be expressed as follows [18]:

$$(\dot{\varepsilon}_s)^m \cdot t_r = C \tag{2}$$

where m and C are material constants. The logarithmic form of Eq. 2 is graphically represented in Fig. 7. It is clear that the experimental data have a reasonable agreement in the case of MAR-M 302. The modified Monkman–Grant equation is written as [19]:

$$t_t = K\dot{\varepsilon}_s^m \tag{3}$$

where the time to tertiary creep, t_t, is the sum of the primary and secondary creep lives $(t_p + t_s)$; m and K are material constants. Time to tertiary creep versus minimum creep rate for MAR-M 302 samples are shown in Fig. 8. Its is evident that modified Monkman–Grant equation is in fair agreement with experimental data.

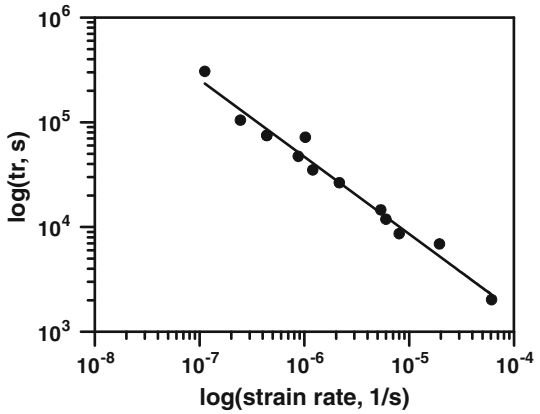

Fig. 7 Graphical representation of Monkman–Grant equation for MAR-M 302

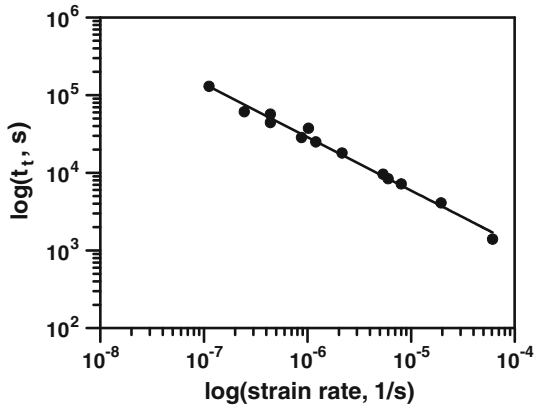

Fig. 8 Time to tertiary creep versus minimum creep rate in MAR-M 302

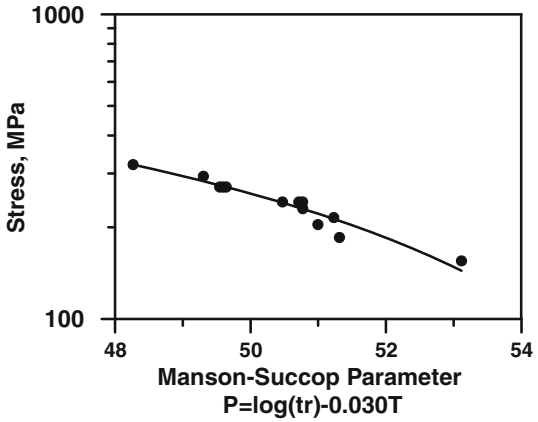

Fig. 9 Manson–Succop parametric curve

The method of Manson–Succop is based on the parallelism of the iso-stress lines, with same slope B, in a graph $\log(t_r)$ versus T, in the following way [20]:

$$P_{MS} = \log(t_r) - BT \tag{4}$$

where t_r is rupture time, T temperature, and B is a constant. Figure 9 shows the Manson–Succop parametric curve for MAR-M 302. The Orr–Sherby–Dorn life prediction method is on the basis of a parameter that is derived by considering the expression for the secondary creep strain rate at constant stress [21]:

$$P_{OSD} = \log t_r - \frac{Q}{RT} \tag{5}$$

where t_r is the time to rupture at temperature T, Q is a characteristic activation energy for the process, and R is the universal gas constant. The Larson–Miller parameter is defined as [22]:

$$P_{LM} = T(\log t_r + C) \tag{6}$$

where C = L–M constant = 20 for many materials, T = test temperature in K, and t_r = time to rupture in hours. The values of C range from 15 to 26 for many materials. The constant for MAR-M 302 has not been reported, but is typically about 20 for many Ni-base superalloys [23–26]. In the present investigation constant value of $C = 18.4$ offered the highest degree of fit for MAR-M 302. Figure 10 shows the Sherby–Dorn and Larson–Miller parameter diagrams for MAR-M 302 superalloy.

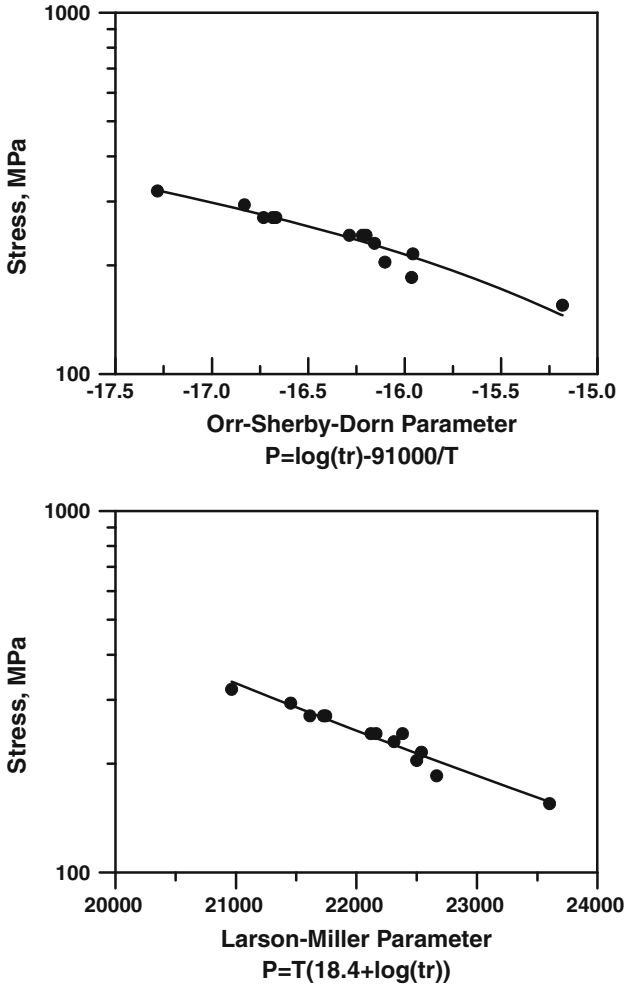

Fig. 10 The Orr–Sherby–Dorn and Larson–Miller parameter diagrams

Discussion

Constitutive equations

Concerning creep behavior modeling, many constitutive equations have been proposed [16, 27]. These equations describe creep curves up to the secondary and/or tertiary stage. The constitutive creep equations that are widely accepted as basic equations are as following [28, 29].

$$\varepsilon_c = at^b \quad \text{Power law} \tag{7}$$

$$\varepsilon_c = \varepsilon_0 + a\{1 - \exp(-bt)\} \quad \text{Exponential law} \tag{8}$$

$$\varepsilon_c = \varepsilon_0 + a\ln(1 + bt) \quad \text{Logarithmic law} \tag{9}$$

$$\varepsilon_c = \varepsilon_0 + a\{1 - \exp(-bt)\} + c\{1 - \exp(-dt)\} \quad \text{Blackburn} \tag{10}$$

where ε_c is a creep strain and t is a time. ε_0, a, b, c, and d are constants obtained from analysis. Since ε_c is a creep strain, it does not include instantaneous strain. Consequently, ε_0 is not an instantaneous strain and it is used, except for power law, for the purpose of improvement of fitting accuracy. Results of regression analysis on creep strain versus time curves and creep rate versus time curves are shown in Figs. 11 and 12, respectively. Concerning primary and secondary creep stages, it appeared that all the equations accurately reproduce creep curves. However, the

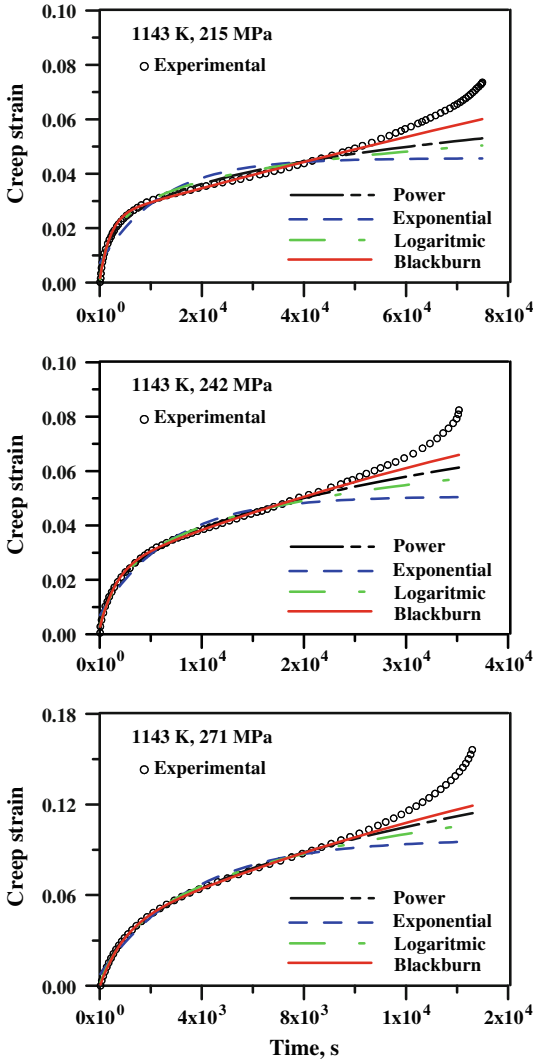

Fig. 11 Results of regression analysis on creep strain versus time curves for MAR-M 302

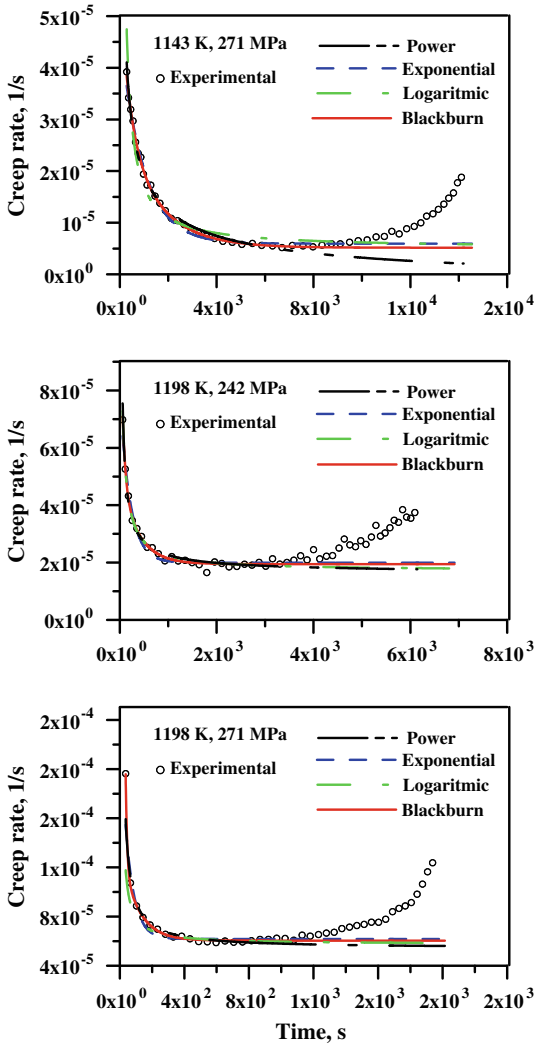

Fig. 12 Results of regression analysis on creep rate versus time curves for MAR-M 302

curve predicted by the Blackburn's equation reproduces the experimental data well, even at the beginning of primary creep.

Kinetic analysis

Creep rupture is usually caused by thermally activated time dependent plastic deformation. The creep behavior is a function of temperature, stress, structural factor, and chemical compositions, etc. [16]. Concerning creep as thermally activated phenomenon, it can be expressed using the following empirical equation [30, 31].

$$\dot{\varepsilon} = A\sigma^n \exp\left(-\frac{Q}{RT}\right) \tag{11}$$

where $\dot{\varepsilon}$ is the minimum strain rate, A is a constant, σ the engineering stress, n the stress exponents for creep, R the universal gas constant, T the absolute temperature, and Q is the activation energy for creep. Activation energy for creep, Q, can be derived as:

$$Q = -R\left(\frac{-\partial \ln \dot{\varepsilon}}{\partial T^{-1}}\right)_{\sigma} \tag{12}$$

Figure 13 shows the variation of creep rate with $1/T$. It is clear the calculated activation energy for MAR-M 302 increased with increasing stress. This behavior indicates that at the imposed temperatures (1073–1273 K) lattice or volume diffusion would be dominant. Concerning Dorn creep equation,

$$\dot{\varepsilon} = A\frac{DGb}{RT}\left(\frac{\sigma}{G}\right)^n, \tag{13}$$

where A and n are constants, D diffusion coefficient, G shear modulus, and b is Burgers' vector, it is convenient to

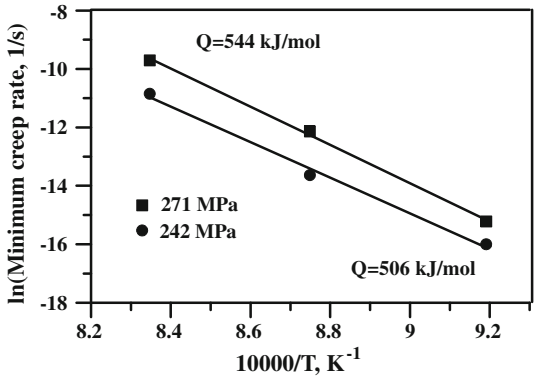

Fig. 13 The variation of creep rate with $1/T$

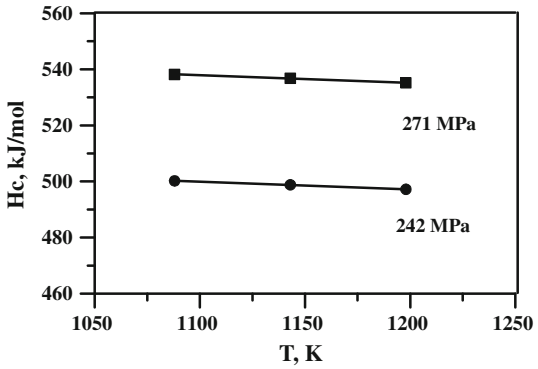

Fig. 14 The variation of activation enthalpy for creep, H_c, with creep temperature

define an activation enthalpy for creep, H_c, which does not contain terms arising from either G or T [32]:

$$H_c = Q_c - RT\left[\frac{n\beta\left(\frac{T}{T_m}\right) - 1}{1 - \beta\left(\frac{T}{T_m}\right)}\right] \tag{14}$$

where β is a material constant with a normal range of 0.35–0.55, Q_c is activation energy for creep and n is stress exponent in Dorn equation. Assuming $\beta = 0.45$ and $n = 5$ [32] the variation of H_c with temperature for MAR-M 302 is shown in Fig. 14. It can be observed that the calculated activation enthalpy increased with increasing stress and slightly decreased with increasing temperature.

Based on Eq. 11 the dependence of creep rate on the applied stress, called stress exponent n, can be calculated:

$$n = \left(\frac{\partial \ln \dot{\varepsilon}}{\partial \ln \sigma}\right)_T \tag{15}$$

Figure 15 shows the dependence of steady state creep rate on the applied stress in which the stress exponent decreased with increasing test temperature.

The results obtained in this study showed that the stress exponent n and the activation energy for creep (Q) vary as the test conditions are changed. This is consistent with the other

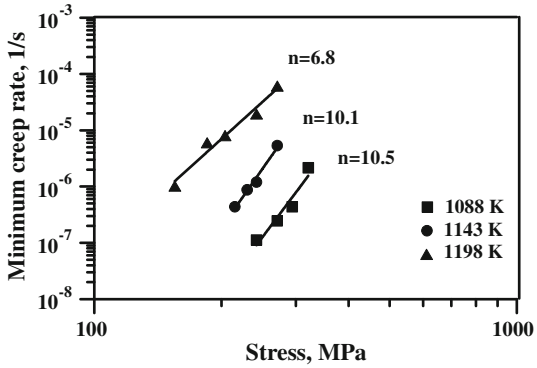

Fig. 15 The dependence of steady state creep rate on the applied stress

reported observations. For instance, over the stress ranges covered for Gr. 122 steel [33, 34], a decrease from $n \approx 16$ to $n \approx 5$ is observed on increasing the test temperature from 823 to 1023 K, with Q varying from 680 to 500 kJ/mol. For the same steel, a change has also been reported from $n \approx 60$ and $Q = 1045$ kJ/mol at high stresses towards $n \approx 5$ and $Q = 640$ kJ/mol at low stresses [35]. These anomalously variable values of n and Q are typical of the results obtained for particle-hardened alloys [36].

Creep rupture life prediction

Monkman–Grant (Eq. 2) and modified Monkman–Grant (Eq. 3) creep life prediction methods are based on the relationship between the secondary or steady state creep rate and rupture life. Based on the results obtained (Figs. 7, 8) a linear regression program was used and the constants for Monkman–Grant ($m = 0.74$, $C = 1.79$) and modified Monkman–Grant ($m = -0.69$, $K = 2.05$) equations were determined. The calculated value of m is close to other reported results. For 0.3% carbon steel and 2.25Cr–1Mo steel, exponent m in Eq. 2 was evaluated to be 1, indicating that the time to rupture is inversely proportional to the minimum creep rate. The value of m for the other materials is lower than 1; $m = 0.78$, 0.66, and 0.60 for 12Cr–1Mo–1W–0.3V steel, 18Cr–8Ni austenitic steel, and Ni-base superalloy U500, respectively [37].

As suggested by Ashby and Dyson [37], the Monkman–Grant parameter C in Eq. 2 depends on total elongation. Abe [15] has also suggested that the constant C denotes the ratio of time to rupture to the duration of the accelerating creep region:

$$C = t_r/(t_r - t_m) \tag{16}$$

where t_m and t_r are the onset time of acceleration creep and rupture time, respectively. The value of C based on Eq. 16 for MAR-M 302 was calculated to be 3.07 ± 0.3.

The life prediction methods of Orr–Sherby–Dorn, Larson–Miller, and Manson–Succop are based on the

iso-stress lines in a graph with coordinates $\log(t_r)$ versus $1/T$ or T (t_r, rupture time, T, test temperature) [20]. The results obtained in the present analysis showed that the Larson–Miller and the Orr–Sherby–Dorn life prediction techniques (Fig. 10), exhibited equivalent results and the Manson–Succop parametric curve (Fig. 9) offered the lowest degree of fit. Due to the limited amount of creep data obtained in the present work of relatively short durations it is difficult to attribute any reason why the Manson–Succop methods showed the worst results.

As demonstrated by Pink [38], none of the extrapolation methods are based on consistent physical hypothesis and their relative efficiency depends on the circumstantial conditions of stress and temperature [15]. The Larson–Miller method is in agreement with the theoretical equation for low temperature deformation only and cannot describe the high temperature properties accurately [38]. Furthermore, the Larson–Miller method is a reliable technique for life prediction as long as the alloy microstructure is stable during prolonged exposure at high temperature [39]. The Manson–Succop method has no physical basis, but manages to express well the creep rupture behavior in a higher temperature range [38]. In this investigation, the reliability of the Manson–Succop, Larson–Miller, and Orr–Sherby–Dorn techniques were fairly equivalent and it seems that more results are needed to confirm the superiority of the one method for MAR-M 302 alloy creep data.

Conclusions

- Various constitutive equations were fit using MAR-M 302 creep data. The Blackburn equation offered the highest degree of fit among constitutive equations employed in this study.
- The Larson–Miller and the Orr–Sherby–Dorn life prediction techniques, exhibited equivalent results and the Manson–Succop parametric curve offered the lowest degree of fit.
- The minimum creep rate and the rupture time are related by the Monkman–Grant $\left((\dot{\varepsilon}_s)^m \cdot t_r = C\right)$ and modified Monkman–Grant $\left(t_t = K\dot{\varepsilon}_s^m\right)$ relations, with an absolute m value close to 0.7.

References

1. Klarstrom DL (1994) In: Koul AK, Immarigeon JP, Wallace W (eds) Advances in high temperature structural materials and protective coatings. National Research Council of Canada, Ottawa, Canada, p 54
2. Davies R (ed) (1997) ASM specialty handbook, heat resistant materials, metallurgy, processing and properties of superalloys. ASM International, Materials Park, OH, pp 221–254
3. Beltra AM (1987) In: Sims CT, Stoloff NS, Hagel WC (eds) Superalloys II. John Wiley & Sons, New York, p 135
4. Chen LJ, Liaw PK, Hel YH, Benson ML, Blust JW, Browning PF, Seeley RR, Klarstrom DL (2001) Scr Mater 44:859
5. Tang C, Pan F, Qu X, Duan B, Wang T, He X (2008) Rare Metals 27:292
6. Jiang WH, Guan HR, Hu ZQ (1999) Mater Sci Eng A271:101
7. Szala J, Szczotok A, Richter J, Cwajna J, Maciejny A (2006) Mater Charact 56:325
8. Jiang WH, Guan HR, Hu ZQ (1999) Metall Mater Trans 30A:2251
9. Kim D, Kim J, Sa J, Lee Y, Park C, Moon S (2008) Mater Sci Eng A 483–484:262
10. Yao H, Xuan F, Wang Z, Tu S (2007) Nucl Eng Des 237:1969
11. Swindemana RW, Swindeman MJ (2008) Int J Press Vessel Pip 85:72
12. Beck CG, Santhanam AT (1978) Scr Metall 12:255
13. Baufeld B, Tzimas E, Müllejans H, Peteves S, Bressers J, Stamm W (2001) Mater Sci Eng A315:231
14. Jiang WH, Yao XD, Guan HR, Hu ZQ (1999) Metall Trans A 30A:513
15. Abe F (2008) Int J Press Vessel Pip 85:99
16. Viswanathan R (1989) Damage mechanisms and life assessment of high-temperature components. ASM International, Ohio, p 59
17. Monkman FC, Grant NJ (1956) Proc ASTM 56:593
18. Sordi VL, Bueno LO (2008) Mater Sci Eng A 483–484:498
19. Koul AK, Castillo R, Willett K (1984) Mater Sci Eng 66:213
20. Bueno LO, Sordi VL (2008) Mater Sci Eng A 483–484:560
21. Orr R, Sherby OD, Dorn JE (1954) Trans ASME 46:113
22. Larson FR, Miler J (1952) Trans ASME 74:756
23. Gu YF, Cui C, Ping D, Harada H, Fukuda T, Fujioka J (2009) Mater Sci Eng A510–511:250
24. De Cicco H, Luppo MI, Gribaudo LM, Ovejero-García J (2004) Mater Charact 52:85
25. Scholz A, Wang Y, Linn S, Berger C, Znajda R (2009) Mate Sci Eng A510–511:278
26. Hou JS, Guo JT, Zhou LZ, Yuan C, Ye HQ (2004) Mater Sci Eng A374:327
27. Kassner ME, Pérez-Prado M (2004) Fundamentals of creep in metals and alloys. Elsevier Ltd, Oxford
28. Sawada K, Tabuchi M, Kimura K (2009) Mater Sci Eng A510–511:190
29. Holdsworth S (2004) Mater High Temp 21:25
30. Garofalo F (1965) Fundamentals of creep and creep rupture in metals. MacMillan, New York
31. Ray AK, Diwakar K, Prasad BN, Tiwari YN, Ghosh RN, Hittenberger JD (2007) Mater Sci Eng A 454–455:124
32. Bird JE, Mukherjee AK, Dorn JE (1969) In: Brandon DG, Rosen A (eds) Quantitative relation between properties and microstructure. Israel University Press, Jerusalem, p 255
33. Kimura K (2005) In: Shibli IA, Holdsworth SR, Merckling G (eds) Creep and creep fracture in high temperature components–design and life assessment issues. DEStech Publ, Lancaster, PA, p 1009
34. NIMS (2006) Creep Data Sheet No: 51
35. Maruyama K, Lee JS (2005) In: Shibli IA, Holdsworth SR, Merckling G (eds) Creep and creep fracture in high temperature components–design and life assessment issues. DEStech Publ, Lancaster, PA, p 372
36. Evans RW, Wilshire B (1985) Creep of metals and alloys. Institute of Metals, London
37. Ashby MF, Dyson BF (2002) In: Mishra RS, Earthman JC, Raj SV (eds) Proceedings of TMS symposium on creep deformation: fundamentals and applications. Seattle, USA, p 309
38. Pink E (1994) Mater Sci Technol 10:340
39. Marahleh G, Kheder ARI, Hamad HF (2006) Mater Sci Eng A433:305